Digital Receiver For Interference Suppression in Microwave Radiometry

J. T. Johnson, N. Niamsuwan, and S. W. Ellingson[1]
The Ohio State University ElectroScience Laboratory
1320 Kinnear Rd., Columbus, OH 43212
johnson.1374@osu.edu
[1] Department of Electrical and Computer Engineering
Virginia Tech

***Abstract*— Recent results are reviewed from an IIP project on the development of digital backends for microwave radiometer systems. The digital backends developed implement real-time RFI suppression algorithms for interferers localized in either time or frequency. Results from ground and airborne experiments at L- and C-bands are described that indicate the advantages of digital receivers in reducing RFI effects on measured brightnesses.**

I. Introduction

Microwave radiometry can be severly impacted by radio frequency interference. Under the support of the NASA IIP program, a project at The Ohio State University has developed digital receiver backend technologies in order to improve the removal of RFI from observed brightnesses. Results of this project are described in this paper. Section II discusses RFI issues for microwave radiometers, while Section III reviews the digital backends developed under the IIP program. Section IV then describes RFI surveys completed as part of the project, and Section V provides a summary of the ground and airborne experiments performed.

II. RFI Issues for Microwave Radiometers

The design of a traditional microwave radiometer is based on the assumption that the observed signal consists only of thermal noise. Because the goal of radiometry is to estimate accurately the mean power of the incoming thermal noise, long integration periods (on the order of milliseconds or longer) are desirable in order to reduce uncertainty. Only the mean power estimate after this integration period is of interest, so a traditional radiometer will not record information within an integration period. In addition, the use of large bandwidth channels is desired in order to further reduce uncertainty in the estimate of mean power. Because naturally emitted thermal noise varies very slowly with frequency in most cases, measurements from channels with similar center frequencies are deemed identical, and single channel observations are sufficient to represent a large portion of the spectrum.

A traditional "direct detection" radiometer block diagram is illustrated in Figure 1; the front end filter here typically includes a large bandwidth (10's or 100's of MHz), while the low pass filter integrates the power up to millisecond scales before digitization.

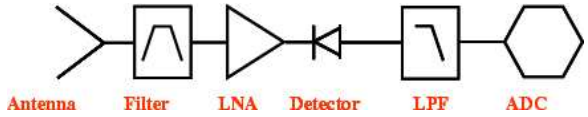

Fig. 1. Block diagram of traditional radiometer system

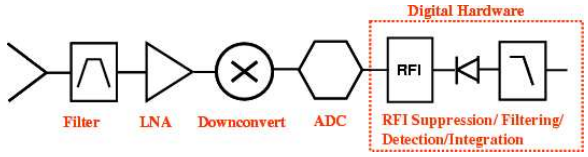

Fig. 2. Block diagram of new radiometer system

The addition of RFI to the observed channel violates the noise-only assumption, and causes serious problems for a traditional radiometer. Although interference can take a variety of forms, in many cases RFI may be expected to be localized either in time (i.e. pulsed type interference) or frequency (narrowband interference), or in both domains. If only a small number of such "localized" interfering sources are present, a large portion of either the observation time or bandwidth may contain no interference. However, the traditional radiometer is unable to separate the corrupted and uncorrupted portions of the observation, and therefore may produce corrupted data even with only limited RFI. Because RFI will always increase the mean power when compared to that of the geophysical background, post-processing of the data can be applied to eliminate abnormally high observations. However, lower level RFI can be difficult to separate from geophysical information, making parameter retrievals problematic. Note that an interferer with a large amplitude but small temporal duty cycle and/or small bandwidth may appear as low level RFI when averaged over time and frequency.

A simple way to extend the RFI mitigation capabilities of the traditional radiometer is to increase either the temporal sample rate or the number of frequency channels in the system. These approaches can be implemented in an analog fashion by simple extensions of the traditional radiometer, and the complete data set recorded for post-processing to eliminate RFI at finer temporal and spectral resolution. However, the number of channels that can be implemented using an analog

approach is limited, given that additional hardware must be added for each new channel. The temporal sampling rate that can be achieved is also limited by both the RF hardware and the data acquisition subsystem, since the amount of data to be stored eventually becomes unmanageable. Use of digital receiver technologies can address some of these issues: the implicit high temporal sampling rate of a digital receiver allows temporally localized sources to be resolved. In addition, an FFT operation can be performed in real time to obtain a much larger number of frequency channels than is possible using analog sub-channels. However, the data rate of such a system is also much larger than that of the analog approaches. To reduce the data rate, an RFI mitigation processor can be added to the digital receiver to implement simple time and/or frequency domain mitigation algorithms in real time. The resulting "RFI-free" data is then integrated over time and/or frequency to produce a manageable final output data rate.

The digital receiver developed under the IIP project is based on such an architecture. Figure 2 illustrates this configuration; note a downconversion stage is included given that directly sampling the incoming RF energy may be difficult due to analog-to-digital converter (ADC) limitations. Direct RF sampling has been utilized in L-band radiometry previously [1], but the receiver prototypes developed in the current project include downconversion stages.

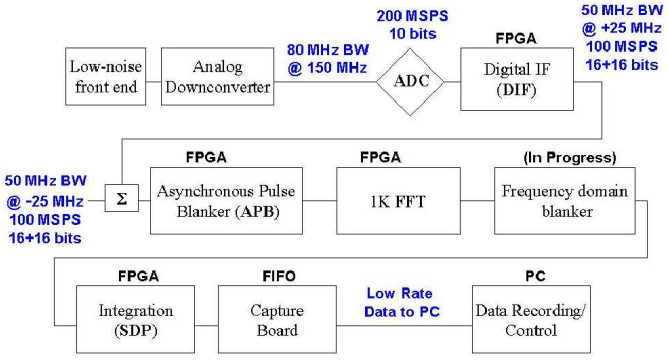

Fig. 3. Block diagram of radiometer

III. System overview

Figure 3 presents a more detailed block diagram of the microwave radiometer system developed [2]-[3]. The basic design consists of a standard radiometer frontend, an analog downconverter section, and a digital backend unit capable of coherently sampling a 100 MHz bandwidth. A bandwidth of 100 MHz was chosen for the system based on a compromise between available digital technology and a desire for large bandwidth operations. At L-band, this bandwidth includes the 20 MHz of protected spectrum, as well as other spectral regions more likely to contain RFI sources. The same digital backend system (i.e. after the downconversion stage) can be utilized at an arbitrary RF frequency simply by modifying the antenna, front end, and downconversion stages.

It is desirable to include a large number of bits in the sampling process in order to resolve both environmental noise and RFI contributions without encountering dynamic range problems. A survey of available ADC's at the beginning of the project showed that a sample rate of 200 MSPS (so that 100 MHz is the maximum bandwidth resolvable) with 10 bits was the limit of easily available technology as of early 2002. Using a large number of ADC bits opens the possibility of reduced gain in the radiometer frontend and downconverter sections, as higher dynamic range is typically achieved in ADC's by increasing sensitivity (i.e. lowering the power required to toggle the lowest ADC bit.) Reduced gain is desirable in general in order to improve receiver stability, and thereby potentially reduce thermal control requirements throughout the entire system. Trade-off studies of receiver stability versus gain were not performed under the IIP project however.

Although resolving 100 MHz with one such ADC would be possible, it was deemed preferable to utilize 2 ADC's sampling 50 MHz each so that digital filtering could be incorporated into the RFI processor to limit receiver bandwidth digitally. Use of digital filters is desirable due to possible stability issues of analog filters with temperature and other environmental variations, particularly near the cutoff frequencies of the filter response. The design developed keeps the analog filter passband wider than that ultimately set by the digital filters, so that the near cutoff regions of the analog filters do not contribute significantly to the observed bandwidth.

Accordingly, the 100 MHz bandwidth is split into 2 50 MHz channels, and each channel is then sampled at 200 MSPS using 10 bits. The resulting digital data of each channel is centered at 50 MHz and is spectrally reversed due to the use of the second ADC Nyquist zone. The "Digital IF" (DIF) FPGA module downconverts each channel to 0 Hz (so now the samples are complex-valued), digitally filters each to 50 MHz bandwidth, decimates by 2, and then up- or down-converts the two channels to center frequencies of +/-25 MHz (still complex). Finally both channels are added so that -50 to 50 MHz data emerges from the DIF module in 16-bit "I"+16-bit "Q" format at 100 MSPS.

Following the DIF output is a cascade of FPGA modules which can be programmed to perform a variety of functions. The strategy used in the current project is as shown in Figure 3: mitigation of radar pulses using "asynchronous pulse blanking" (APB), channelization into 100-kHz bins using a 1K FFT, and integration to generate power spectra.

The APB [4]-[5] is designed to detect and blank radar pulses, which often are the dominant source of external L-Band RFI below 1400 MHz. Typical radar pulses range from 2-400 μs in length and occur 1-75 ms apart [6], illustrating the low temporal duty cycle of these sources. To detect these pulses, the APB maintains a running estimate of the mean and variance of the sample magnitudes. Whenever a sample magnitude greater than a threshold number of standard deviations from the mean is detected, the APB blanks (sets to zero) a block of samples beginning from a predetermined period before the triggering sample, through and hopefully including any multi-path components associated with the detected pulses. APB operating parameters are adjustable and can be set by the user.

Following the APB is a length-1K complex FFT, which achieves approximately 98% duty cycle in performing the FFT computations. A triangular window is applied before the FFT. Considered but not implemented in the hardware of this project is a frequency domain blanking module, which is similar in concept to the APB, except applied independently to each frequency bin. The FFT output is processed through a "spectral domain processor" (SDP) module which computes the magnitude-squared for each frequency bin and computes a linear power average over many FFT outputs. Calibration corrections for the blanking operation are incorporated by recording the number of blanked samples included in an SDP integration period. The SDP module is also capable of computing a max-hold operation in RFI detection applications. Results from the SDP are passed at a relatively low rate to a PC via a "capture" interface system. Total power can be computed by summation of frequency bins within the digital hardware, or the same process can be implemented in software for increased flexibility in removing RFI across frequency.

A. Receiver prototypes developed

Over the course of the project, three prototype digital receivers have been completed; photographs of these receivers are available in [7]. The first, LISR1, included only one ADC and therefore sampled only a 50 MHz bandwidth, but retained the full DIF, APB, FFT, and SDP operations with a few exceptions. The FPGA components utilized in this prototype also were insufficient in size to allow a full duty cycle FFT operation. This resulted in only a 14% duty cycle for the final observations. LISR1 also included no APB calibration corrections and no possibility of max-hold computations. LISR1 was completed by late September 2002, and was utilized in the Arecibo observation campaign discussed in Section V-A.

A second prototype, LISR2, was developed to remove the limitations of LISR1; Figure 4 is a photograph of the LISR2 digital backend. LISR2 included both ADC components, so that full 100 MHz observations were achieved. A higher-density series of FPGA components were also used (the Altera "Stratix" line), allowing parallel FFT processors to be included so that 98% duty cycle computations resulted. The LISR2 FPGA program was also improved to include the max-hold operation. However, the APB scaling operation still remained difficult with LISR2 due to the presence of the APB and SDP components on separate FPGA cards. An ethernet interface to LISR2 allows operation of the system in several modes, including a direct recording of raw sampled ADC data, power integration with the APB on or off, as well as max-hold operations with the blanker on or off. LISR2 was completed by late April 2003, and utilized in local observations, as well as in airborne observations at C-band.

A final prototype, LISR3, was developed to improve communication among separate components (i.e. DIF, APB, FFT, SDP) of the system. In particular, the APB calibration correction requires use of APB blanking information in the integration computation. A larger "Stratix" component was chosen to allow the entire processor to reside within a single FPGA. LISR3 was completed by late March 2005 and enabled accurate APB calibration corrections to be achieved.

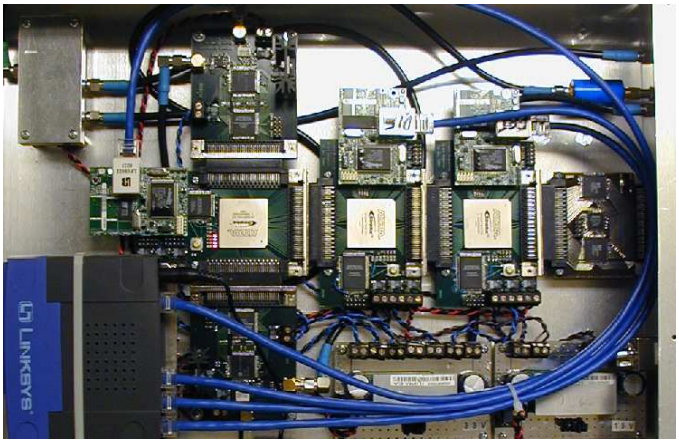

Fig. 4. LISR2 digital backend; the vertical cascade of three circuit boards near the left hand side contains the dual ADC sections (upper and lower boards) and the digital channel combination and filtering (DIF) section (center board). The APB section for removing temporal pulses is also implemented on the center board. Following the vertical cascade to the right is the FFT processor, then the SDP section for power computation and integration operations. Finally a "capture card" provides the interface to the PC. Microcontrollers are also included on each card (the smaller attached circuit boards with ethernet cables) to enable PC setting of FPGA parameters through an ethernet interface.

IV. RFI SURVEYS, LISA CAMPAIGN, AND ALGORITHM TESTING

A. Local RFI surveys

A crucial aspect of system testing involves the RFI environment in which the tests are performed. Local tests at The Ohio State University ElectroScience Laboratory experience L-band RFI sources in the local region, so understanding these sources was important for monitoring performance. Accordingly, analytical and measurement studies of the local RFI environment were performed in 2002. Results showed a relatively quiet spectrum in the region 1325-1425 MHz, although a strong pulsed interferer was identified. This interferer is an air-route surveillance radar (ARSR), transmitting pulses of approximately 1μsec duration every 3 msec, located approximately 43 km from the laboratory in London, OH. This source provides an excellent pulsed interferer for assessing APB performance in local measurements. Additional more-continuous narrowband RFI sources have also been observed in the local environment; see [7] for data illustrating these sources.

B. LISA

Although the local OSU environment is likely somewhat representative of other ground-based L-band RFI environments, it was decided early in the project period that airborne L-band RFI surveys in a variety of environments would be highly desirable. Such surveys could provide data for evaluating RFI mitigation algorithm performance against a larger set of sources than those experienced locally. In addition, it is to be expected that RFI power levels are larger in airborne than in ground-based observations, due to more rapidly increasing path loss encountered for ground-based versus free-space paths.

Fig. 5. The LISA equipment rack installed on the P-3.

Accordingly, the L-band Interference Surveyor/Analyzer (LISA) was developed as part of the IIP project to perform these observations [8]-[10]. Because the first deployment of LISA occurred early in the project (January 2nd, 2003), it was necessary to develop the LISA system based on digital receiver designs already in existence early in the IIP project period. For this reason, LISA was based on a digital receiver capable only of sampling a 20 MHz bandwidth, and with no on-board RFI processing. However, the raw "capture"data recorded by LISA was ideal for further use in RFI suppression algorithm evaluations. An antenna-front end system, downconversion unit, and interface to a computer were all implemented for airborne observations.

LISA was deployed in a test flight onboard the NASA P-3 aircraft over the Chesapeake bay region on January 2nd, 2003, followed by a cross-US flight to Monterey, CA on January 3rd. A photograph of the LISA equipment rack on the aircraft is provided in Figure 5. LISA then was operated throughout transit to and in the AMSR-E Wakasa Bay cal-val campaign. LISA successfully recorded a large data set of RFI observations tuned throughout the 1300-1700 MHz band. Numerous RFI sources were observed and categorized, as described in [9]-[10]. Unfortunately, the sensitivity of the LISA system was limited due to placement of its antenna in the tail radome of the P-3 aircraft, so that no conclusive information on RFI in the L-band protected spectrum was achieved. However the large data set and variety of RFI environments experienced enabled a more general study of RFI mitigation methods to be performed.

C. Algorithm studies with LISA data

A particular emphasis of the LISA data studies involved performance of the APB algorithm. This algorithm was simulated in software on the LISA capture data, with the simulation code developed to mimic the hardware system behavior as much as possible. Several studies of the algorithm were performed, including tests of the Gaussianity of the data pre- and post-blanking, effects of variations in the APB threshold and blanking window width, as well as the influence of partially blanked frames in the FFT computation. Results of these studies are documented in [11]. These studies resulted in the APB calibration correction procedure utilized in the LISR3 system, as well as improvements in parameter choices for later APB operations. The dataset remains available for future analyses of any new algorithms.

V. System demonstrations

Several demonstrations of the IIP system were performed throughout the project period, involving use of the LISR1, 2, and 3 prototypes. The majority of these observations recorded integrated FFT power outputs measured with the APB processor either on or off. The resulting data can be plotted as a "spectrogram" series, in terms of the power in all 1024 FFT bins versus time. For raw measured data, it is typical to normalize such plots by the average of each bin over time, so that the passband response of the instrument is removed.

Calibration of recorded data in microwave radiometer observations is based on the use of known brightness calibration targets [12]. Such targets ideally are external to the system antenna, so that the influence of all system components including the antenna can be accounted for in the calibration process. Because external calibration requires moving either the target or the antenna so that the antenna observes the calibration target, it is difficult to perform external calibration repeatedly within a short duration of time. However, receiver gain variations over short periods of time can occur that reduce the calibration accuracy of the system in-between external calibrations.

To address these shorter time scale variations, it is typical to include internal calibration sources within microwave radiometer systems as well. These internal loads (noise diodes with known emitted power levels, or microwave terminators at a known physical temperature) serve as standards for correcting receiver gain variations following the location of the internal loads. Including a switch for internal load measurements as close to the antenna as possible is therefore desirable, so that the internal calibration corrects the majority of later system gain variations. However an internal calibration does not yield correct brightness values for antenna measurements, since the antenna response is not included in the correction.

The experiments to be discussed utilized a variety of calibration methods, including observation of raw data only in some cases. Unfortunately a completely calibrated set of observations at L-band was not achieved during the project period; airborne observations at C-band however have yielded a small set of calibrated data, as will be discussed in what follows.

A. Arecibo measurements

An opportunity arose in November 2002 to co-observe with the LISR1 digital backend at the Arecibo radio observatory. Results from these observations are described in [13]-[15]. The front-end and downconversion stages of the Arecibo observatory were used, and no information on an appropriate calibration procedure was available at the time of the measurements. For this reason results again are considered in terms of relative power variations only. Data were collected in the bands 1230-1280 MHz, 1275-1325 MHz, and 1325-1375 MHz (tuned throughout the campaign), using the "capture" mode (i.e. recording of raw ADC samples) as well as integrated data with the APB on or off. Due the presence of several radar systems in the Arecibo vicinity, the APB was found to have a significant impact on reducing RFI in the dataset. Figure 6 illustrates integrated power levels in the band 1325-1375 MHz obtained from 10.7 seconds of LISR1 observations at Arecibo; the upper plot includes data with the APB off, while APB-on results are shown in the lower plot. In addition, the upper curve within each plot is the maximum value for each FFT bin observed during the integration period; the lower curve is the average of all values. Clearly the APB system is dramatically reducing the impact of interferers at 1330 and 1350 MHz (known to be radar sources), especially in the maximum values observed. A detailed study of the capture data and properties of one of the radar sources observed is documented in [13].

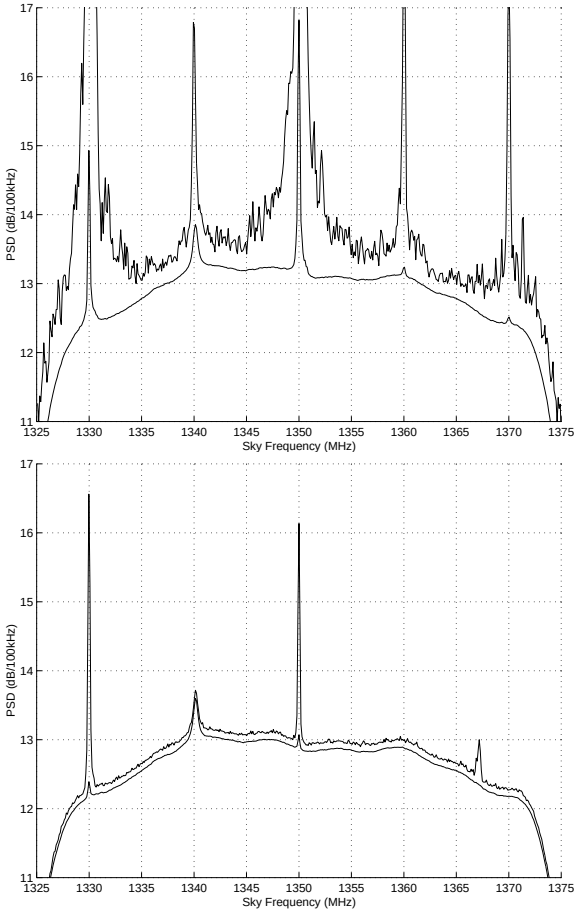

Fig. 6. Sample mean and max-hold spectra from LISR1 observations at Arecibo. See [13]-[15] for more information. *Top Panel:* APB off; *Bottom panel:* APB on.

B. LISR2 Pool campaign

1) Experiment design and system hardware: In order to obtain calibrated brightnesses in a local test, a well defined external calibration procedure is necessary. In addition, a true test would involve three well characterized targets, with the first two targets defining the calibration and the third target being used to evaluate the accuracy of the calibration. It is also desirable to operate such an experiment in the antenna far-field, in order to avoid any complex behaviors of the antenna pattern with range in the near field. An experiment was designed to fulfill these needs involving observations of a large water pool with an antenna on the roof of the ElectroScience Laboratory building. Description of the experiment plan is provided in [12], [16]-[17].

Based on both geometric and far-field considerations, a 1.2 m reflector antenna was selected for the tests. This resulted in a wide antenna pattern, so that filling the antenna pattern completely with the calibration targets was not possible. An alternate approach was pursued based on calibrating only a portion of the antenna pattern, with the remainder of the antenna temperature being considered as system noise. Of course, the stability of this external noise over time is important if an accurate calibration was to be achieved. An antenna and feed were designed, along with appropriately sized water pool and calibration targets (microwave absorbers and reflectors) [18]. An integrated front-end was also designed for this antenna, including switched observations of internal noise diode and terminator sources, as well as both horizontal and vertical polarizations of the antenna. Figure 7 is a block diagram of the final front-end unit used. A photograph of the

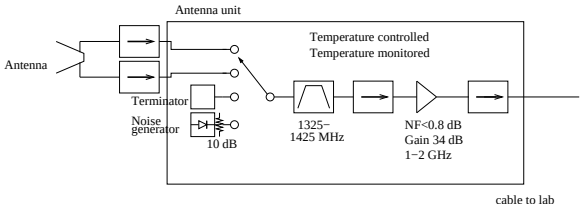

Fig. 7. Block diagram of antenna/front-end unit developed for pool observations

reflector, feed, integrated front-end unit, and antenna mount is provided in Figure 8. These systems along with the external targets were developed during the Spring and Summer of 2003.

2) Results: Experiments began September 2003; Figure 9 includes photographs of the water pool when uncovered, when covered with absorbing loads (the "hot" calibration target) and when covered with reflectors (the "cold" calibration target). The campaign again focused on comparing calibrated integrated brightnesses with the APB either on or off. A calibration cycle, requiring covering the water pool with the absorbers, then reflectors, then uncovered pool observations, could be completed in approximately 40 minutes. The physical temperature of the water pool was monitored during these experiments, as well as that of the ground surrounding the water pool.

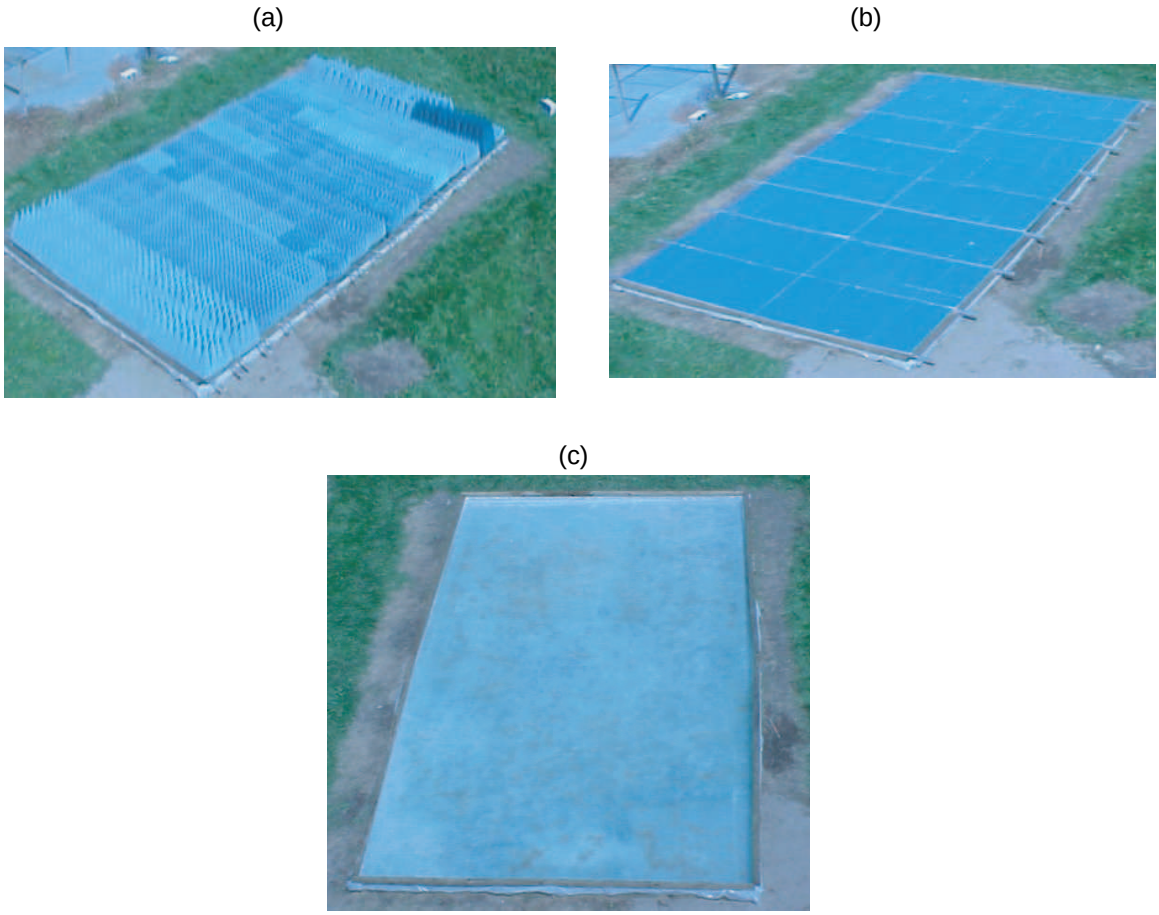

Fig. 9. Water pool (a) covered with absorber (b) covered with reflecting material, and (c) uncovered

Fig. 8. Photograph of antenna deployed on ElectroScience Laboratory roof

Unfortunately, calibrated pool brightnesses obtained from these measurements consistently showed large variations (up to 20-30 K) with frequency in the 1325-1425 MHz band. Such variations are not expected from a water pool target, whose brightness should remain within 1-2 K over this frequency range. Sample results from these campaigns are provided in [7]. The experiments were repeated several times during the period Sept 2003 to Feb 2004 (hampered substantially by the Winter of 2004), but similar problems were found to appear (with differing frequency variations) in each measurement. Modifications of the front-end and downconverter stages performed during this time period yielded no improvement in the calibrated data. Results qualitatively continued to show the impact of the APB on removing the local ARSR influence, and the higher sensitivity obtained due to even an inaccurate calibration revealed the presence of several narrowband interferers within the band of interest.

Analysis of relative power variations observed during the period of an experiment made clear that significant changes in the received power (not uniform across frequency and not identical across all switch ports) were occurring during the period of the measurement. Unfortunately, the configuration of this experiment made separation of internal hardware issues from possible external RFI and/or environmental variations difficult. For this reason an alternate experimental campaign was initiated beginning in Spring 2004.

C. LISR2/3 Sky observations

To address the possible impact of antenna noise contributions from regions outside the area of the pool target previously used, it was decided to utilize up-ward looking sky observations. Because reaching the far-field is not an

issue for sky observations, a much more directive antenna can be used, resulting in reduced contributions from surrounding ground, building, and other environmental noise. Accordingly, a 3 m reflector antenna located in front of the ElectroScience Laboratory was employed; Figure 10 is a photograph of the feed mounted on the antenna.

Tests showed the system's ability to observe astronomical sources, including the moon and hydrogen line emissions from the galactic center. Figure 11 plots relative power variations observed near the 1420.4 MHz hydrogen emission line frequency over a 24 hour period. The "S" shaped curve observed captures the Doppler shift of the hydrogen line as differing portions of galactic emission are observed. The wider emission feature around hour 6 is associated with observations near the galactic center, while the broad increase around hour 14 is associated with the moon entering the antenna pattern. Note these measurements were obtained at extremely high spectral resolution through use of the radiometer "capture" mode: the 256K sample capture (i.e. 2.6 msec of data sampled at 10 nsec) makes possible results in spectral resolutions 256 times narrower than those of the standard system output. Such high spectral resolution is needed to resolve the hydrogen line Doppler shift.

The presence of astronomical sources in sky observations clearly suggests the possibility of a calibration procedure based on the expected brightnesses of such sources. In general, it is expected that the sky provides a slowly varying brightness comprised of known cosmic background, atmospheric, and astronomical source contributions [19]. If a high degree of stability of the system can be demonstrated, sky observations over long time periods should show only a slow evolution as various astronomical sources enter the antenna pattern, while more rapid brightness variations would indicate RFI effects. Overall the goal of the sky observation campaign is to demonstrate reduction of RFI effects, including calibrated information on the number of Kelvins of RFI reduction achieved.

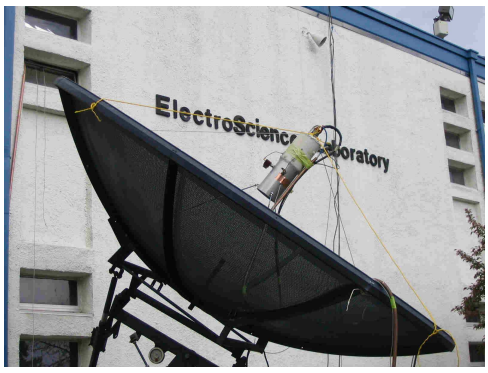

Fig. 10. 3-m diameter parabolic reflector and feed/front-end

As an example of typical measured sky data in a wider bandwidth, Figure 12 illustrates relative power variations in power spectra over 7 hours of observations (00:00 - 7:15am, local time). The color scale represents -0.1 dB to 0.1 dB, so that small variations in relative power levels are illustrated; results staying within these limits over several hours indicate

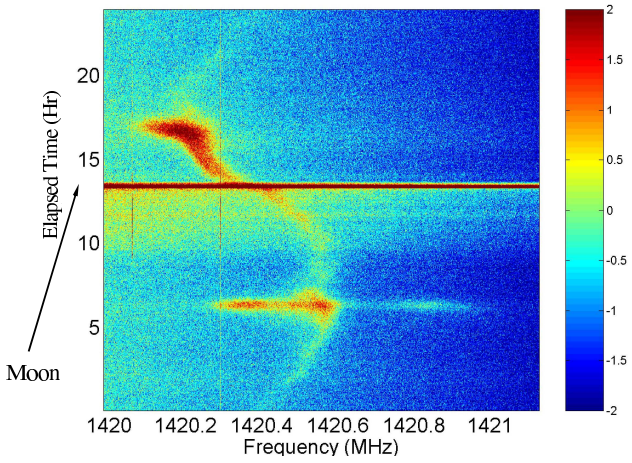

Fig. 11. Relative power variations observed with original 3-m feed near the Hydrogen line frequency

a highly stable system. Plots are normalized by their average over time before conversion to decibels, and results are presented in terms of power spectra (i.e. power outputs of the 1024 point FFT) integrated over 5.3 seconds.

Figure 12-a is the raw noise power of vertically polarized antenna port, with the blanker turned off. Results show a relatively stable behavior, although some long term trends in the relative power across all frequencies are observed, indicating slow variations in the receiver gain. Vertical "streaks" in the figure indicate the presence of frequency localized RFI, where the power varies significantly more than in the RFI-free bins. Strong interferers are observed near 1330 MHz (the ARSR system), 1400 MHz, 1403 MHz, and other frequencies.

Figure 12-b provides a similar plot, but results are illustrated with the blanker turned on. A dramatic reduction in the 1330 MHz source is observed; other non-pulsed RFI sources are not significantly affected.

Figure 12-c plots the results of Figure 12-b in terms of relative power variations after an internal calibration procedure using the noise diode and terminator standards is applied. The long term trends observed in plots (a) and (b) are reduced, indicating that the gain variations observed affect the terminator and noise diode sources in a manner similar to the antenna ports. Some problems in the correction are observed at the band edges and in the cross-over region (1370-1380 MHz) between the two channels, but system stability is otherwise improved through the internal calibration procedure. Efforts to improve these procedures are continuing.

Figure 13 plots relative variations in time of the total power of Figure 12-c. The results were computed from the sum of all frequency channels, with the exception of frequencies near 1400 MHz and 1403 MHz since these bands contain strong narrow-band RFI. Results show total power variations within 0.05 dB over 7 hours of observations. The increase in power observed (the results presented have a negative gain

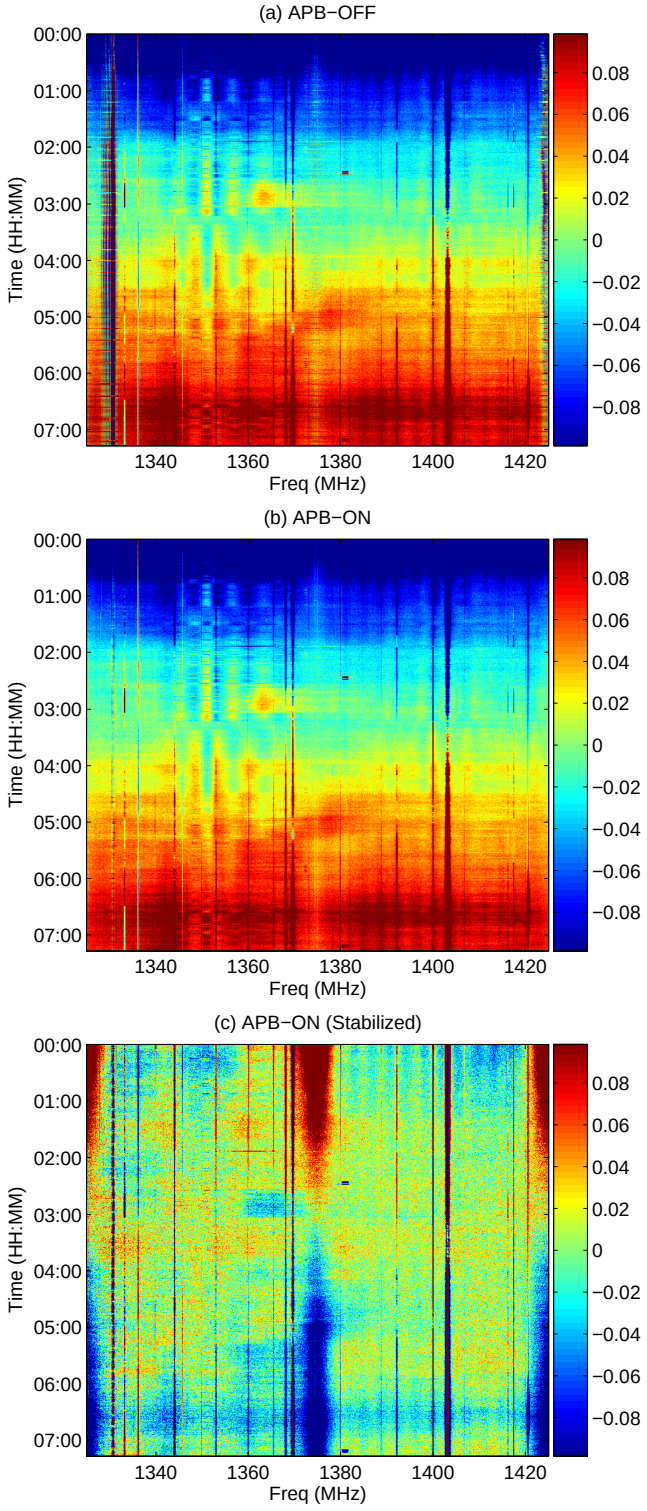

Fig. 12. Relative power in dB, 7-hrs observation, V-Pol antenna port. The antenna was fixed at azimuth angle=154°, polar angle=26.5° (from zenith)

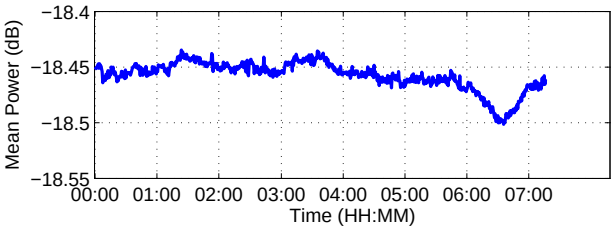

Fig. 13. Relative variations of the internally calibrated total power (i.e. integrated over frequency) in Figure 12-c.

due to the internal calibration procedure) seen at 6:30am corresponds to observation of the galactic plane. The internal calibration procedure (data not shown) shows these variations to be on the order of a few Kelvin. Further processing of these data to exclude other narrowband RFI sources should provide additional information and/or stability, and will continue until a final result is achieved.

D. CISR airborne measurements

1) CISR system design: Though the IIP project focuses on L-band applications, the digital receiver backend developed can be used at other RF frequencies. C-band is another RF frequency of particular concern for RFI corruption, as this band is desirable for soil moisture and sea surface temperature sensing, while there is no protected spectrum available. Recent airborne [20] and satellite data [21] clearly shows RFI corruption of measured data (using the "traditional" radiometer designs described in Section II.) Due to concerns over RFI at C-band as well as current development of the Conical Microwave Imager/Sounder (CMIS) radiometer as part of the National Polar-Orbiting Environmental Satellite System (NPOESS), a project was initiated in August of 2003 to investigate C-band RFI under NPOESS support. In this project, the LISR2 digital backend was operated in conjunction with the Polar Scanning Radiometer (PSR) system of NOAA/ETL [22]. Antenna, front-end, and downconversion stages were provided by the PSR, while the LISR2 backend provides high temporal and spectral resolution RFI observation and mitigation. The complete system was renamed the C-band Interference Suppressing Radiometer (CISR); see [23] for additional information on the combined system.

2) CISR 2004 deployments: CISR was deployed initially in the Soil Moisture Experiment 2004 (August), but problems with the aircraft as well as with the downconversion and backend implementations resulted in only minimal data being obtained. A larger dataset was obtained during a test flight on October 8th, 2004 in the Chesapeake bay region. Analysis of the data under NPOESS support has shown numerous RFI sources encountered, including both pulsed and more continuous emitters [24]. Because the PSR traditional radiometer system (operated simultaneously with digital backend observations) includes 4 analog sub-channels, this dataset provides an opportunity for evaluating RFI mitigation performance of an analog sub-band approach versus mitigation with the much higher spectral and temporal resolution digital data. Results show that the analog sub-band approach often yields apparently reasonable RFI suppression in cases where one of the sub-bands is RFI-free, but incomplete removal of RFI when all sub-bands contain RFI. This situation is encountered several times in the measured dataset. Digital backend data on the other hand provide sufficient spectral resolution to identify and remove RFI even in these cases.

3) CISR sample results: The calibration procedure of the PSR front end enables a calibration of the digital backend dataset to be performed. However the tuning process utilized to provide complete observations of 5.5 to 7.7 GHz at C-band [23],[24], as well as the use of several digital backend modes during the flights, complicates the process and results in calibration for only a subset of the measured data. An result demonstrating spectral RFI removal is provided in Figure 14, which plots calibrated brightnesses recorded by the 4 PSR analog sub-band channels during an over-water portion of the October 8th, 2004 flight. These 4 sub-bands correspond to $5.8-6.2$, $6.3-6.7$, $6.75-7.1$, and $7.15-7.5$ GHz, respectively, and remain large bandwidth (approx 400 MHz) channels. Figure 14 also includes results after an RFI removal algorithm [20] is applied to these 4 sub-bands; the algorithm is based on the assumption that the 4 subband brightnesses should be well-fit by a line in frequency. Brightnesses that violate this assumption are deemed corrupted, and replaced with values from channels that are deemed acceptable. This procedure is found to be effective in removing obvious RFI contributions in Figure 14; note that channel four however is not modified, as this channel typically produces the smallest brightnesses throughout this portion of the flight.

The vertical line in Figure 14 marks a particular point where calibrated digital backend data is available within the bandwidth of PSR channel 4. Figure 15 plots calibrated CISR brightnesses at this point, and shows the presence of a strong narrowband source near 7110 MHz. Note data within a few MHz of the CISR band-edges are not reliably calibrated due to reduced gain in the IF passband, and are excluded in the following discussion. Though not shown, data with the APB on showed no impact on this source, indicating this source's slow variation in time. Mean brightnesses for this CISR spectrum were compared to those excluding the RFI region marked between the two vertical lines in Figure 15. Results showed this source to contribute approximately 4 K when scaled to the PSR channel 4 bandwidth. This level of contribution is consistent when comparing the channel 4 data of Figure 14 to sea observations earlier in time. This example clearly demonstrates the advantages of higher spectral resolution in removing RFI, as this narrowband source clearly identifiable as RFI (i.e. brightness greater than 7000 K) in the digital data produces a low-level RFI contribution (i.e. 4 K) to a large bandwidth channel that is much more difficult to separate from geophysical variations.

C-band observations will continue in 2005 under NPOESS support; a journal article documenting results from the October 8th flight is currently in preparation. Efforts to match the observed RFI sources against licensed C-band sources from an NPOESS database have been initiated to assess methods for forecasting RFI levels from such database information.

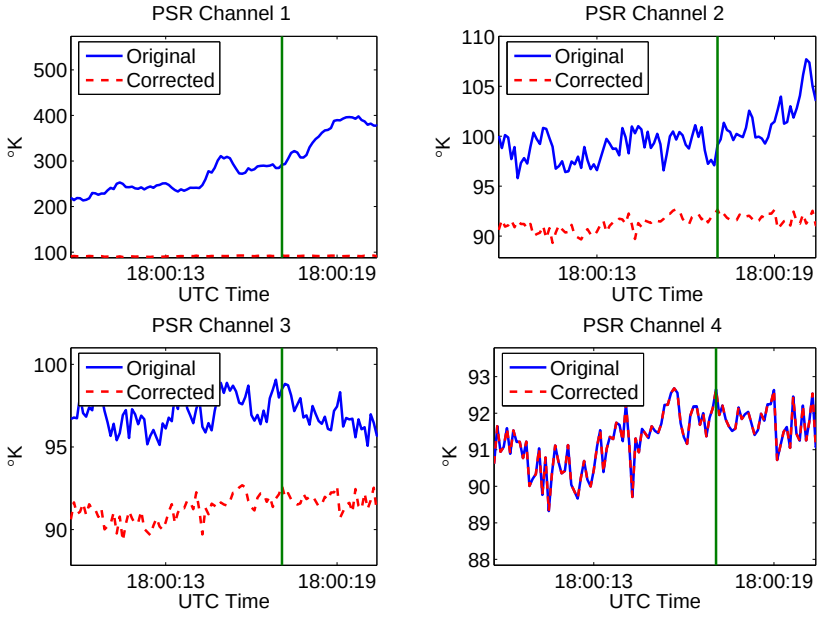

Fig. 14. PSR measured brightnesses versus time during a portion of the October 8th, 2004 test flight. Brightnesses in 4 PSR analog sub-bands are plotted before and after a 4 sub-band RFI removal process [20] is applied.

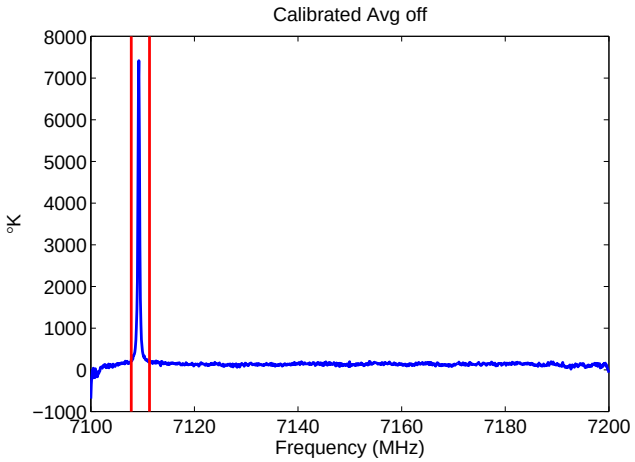

Fig. 15. Calibrated CISR (i.e. digital backend) brightnesses (APB off) measured at the location of the vertical line in Figure 14

VI. Conclusions

Under the support of the NASA IIP program, this project has demonstrated the potential for RFI mitigation in space-borne radiometers through the use of digital receiver backends. Results from the project have qualitatively shown the gains that can be achieved through simple temporal and spectral RFI removal techniques.

It is certain that incorporation of digital receiver technologies into passive remote sensing systems will increase in the future, as such technologies can dramatically improve the capabilities of such systems in mitigating RFI. Other advantages of these systems not explicitly discussed here include potential stability improvements, possible calibration enhancements, as well as more simple and accurate computation of correlations in either polarimetric or interferometric sensors. Evaluation of these gains awaits further studies and the first deployment of these systems in space.

Acknowledgments

This work was supported in part by NASA "Instrument Incubator Program" project NAS5-02001 and by the Integrated Program Office of the National Polar-orbiting Environmental Satellite System (NPOESS). The support of the NOAA ETL PSR group, led by Dr. Albin Gasiewski, is acknowledged for contributions to the C-band dataset.

References

[1] Fischman, M. A. and A. W. England, "Sensitivity of a 1.4 GHz direct-sampling digital radiometer," *IEEE Trans. Geosc. Rem. Sens.* , vol. 37, pp. 2172–2180, 1999.

[2] S. W. Ellingson, "A Design Concept for the IIP Radiometer," project internal report, available at `http://esl.eng.ohio-state.edu/~rstheory/iip/docserv.html`, January 11, 2002.

[3] S. W. Ellingson, "Design Concept for the IIP Radiometer RFI Processor," project internal report, available at `http://esl.eng.ohio-state.edu/~rstheory/iip/docserv.html`, January 23, 2002.

[4] S. W. Ellingson, "Functional Design of the Asynchronous Pulse Blanker (Rev. 1)," project internal report, available at `http://esl.eng.ohio-state.edu/~rstheory/iip/docserv.html`, May 1, 2002.

[5] G. A. Hampson, "Implementation of the Asynchronous Pulse Blanker,", project internal report, available at `http://esl.eng.ohio-state.edu/~rstheory/iip/docserv.html`, June 26, 2002.

[6] Ellingson, S. W., *Characterization of Some L-Band Signals Visible at Arecibo*, Technical Report 743467-2,The Ohio State University Electro-Science Laboratory, February 2003.

[7] J. T. Johnson, N. Niamsuwan, B. Guner, and S. W. Ellingson, Year 3 Annual Review Presentation, available at `http://esl.eng.ohio-state.edu/~rstheory/iip/docserv.html`, April 19th, 2005.

[8] S. W. Ellingson, G. A. Hampson, and J. T. Johnson, "Characterization of L-band RFI and implications for mitigation techniques," *IEEE Geoscience and Remote Sensing Symposium*, conference proceedings, 2003.

[9] S. W. Ellingson and J. T. Johnson, "Airborne RFI Measurements over the Mid-Atlantic Coast using LISA", project internal report, available at `http://esl.eng.ohio-state.edu/~rstheory/iip/docserv.html`, Feb 10, 2003.

[10] J. T. Johnson and S. W. Ellingson,"Airborne RFI measurements using LISA during transit to and in the Wakasa Bay Campaign", project internal report, available at `http://esl.eng.ohio-state.edu/~rstheory/iip/docserv.html` , July 3rd, 2003.

[11] N. Niamsuwan, J. T. Johnson, and S. W. Ellingson, "Examination of a simple pulse blanking technique for RFI mitigation" accepted by *Radio Science*, 2004.

[12] J. T. Johnson, "Initial External Experiment Plan for IIP Radiometer" , project internal report, available at `http://esl.eng.ohio-state.edu/~rstheory/iip/docserv.html`, March 15, 2002.

[13] S. W. Ellingson and G. A. Hampson, "Mitigation of radar interference in L-band radio astronomy," *Astr. Journal Suppl. Ser.*, vol. 147, pp. 167-176, 2003.

[14] G. A. Hampson, S. W. Ellingson, and J. T. Johnson, "Design and demonstration of an interference suppressing microwave radiometer," *IEEE Aerospace Conference*, conference proceedings, 2004.

[15] S. W. Ellingson and G. A. Hampson, "RFI and Asynchronous Pulse Blanking at Arecibo," project internal report, available at `http://esl.eng.ohio-state.edu/~rstheory/iip/docserv.html`, Nov 12, 2002.

[16] J. T. Johnson, "Brightness Temperature of a Flat Water Surface" , project internal report, available at `http://esl.eng.ohio-state.edu/~rstheory/iip/docserv.html`, February 26, 2002.

[17] J. T. Johnson, "Continued External Experiment Plan for IIP Radiometer," project internal report, available at `http://esl.eng.ohio-state.edu/~rstheory/iip/docserv.html`, April 10, 2002.

[18] N. Niltawach and J. T. Johnson, "Reflector Antenna, its Mount and Microwave Absorbers for IIP Radiometer Experiments", project internal report, available at `http://esl.eng.ohio-state.edu/~rstheory/iip/docserv.html`, May 8, 2003.

[19] D. M. LeVine and S. Abraham, "Galactic noise and passive microwave remote sensing from space at L-band," *IEEE Trans. Geosc. Rem. Sens.*, vol. 42, pp. 119-129, 2004.

[20] Gasiewski, A. J., M. Klein, A. Yevgrafov, and V. Leuski, "Interference mitigation in passive microwave radiometry," *IGARSS'02* conference proceedings, 2002.

[21] Ellingson, S. W. and J. T. Johnson, "A polarimetric survey of radio frequency interference in C- and X-bands in the continental United States using WindSAT radiometry," submitted to *IEEE Trans. Geosc. Rem. Sens.*, 2004.

[22] Polar Scanning Radiometer web site, `http://www.etl.noaa.gov/technology/psr` .

[23] J. T. Johnson, A. J. Gasiewski, G. A. Hampson, S. W. Ellingson, R. Krishnamarachi, and M. Klein, "Airborne radio frequency interference studies at C-band using a digital receiver," *IEEE Geoscience and Remote Sensing Symposium*, paper in conference proceedings, 2004. (available at `http://www.ece.osu.edu/~johnson/cisr`)

[24] "Airborne RFI measurements with PSR/CXI and CISR in the Chesapeake Bay Region: Initial Data Examination," project technical report, 2004. (available at `http://www.ece.osu.edu/~johnson/cisr`)